BBA - Biomembranes 1864 (2022) 184018

Contents lists available at ScienceDirect

BBA - Biomembranes

journal homepage: www.elsevier.com/locate/bbamem

Persistent organic pollutants in model fungal membranes. Effects on the activity of phospholipases

Paulina Perczyk [a], Maja Młyńczak [a], Paweł Wydro [b], Marcin Broniatowski [a,*]

[a] Department of Environmental Chemistry, Faculty of Chemistry, Jagiellonian University in Kraków, Gronostajowa 2, 30-387 Kraków, Poland
[b] Department of Physical Chemistry and Electrochemistry, Faculty of Chemistry, Jagiellonian University in Kraków, Gronostajowa 2, 30-387 Kraków, Poland

ARTICLE INFO

Keywords:
Model fungal membranes
Persistent organic pollutants
Phospholipases
Langmuir
Monolayers
Brewster angle microscopy
Grazing incidence X-ray diffraction

ABSTRACT

Soils are the final sink for multiple organic pollutants emitted to the environment. Some of these chemicals which are toxic, recalcitrant and can bioaccumulate in living organism and biomagnify in trophic chains are classified persistent organic pollutants (POP). Vast areas of arable land have been polluted by POPs and the only economically possible means of decontamination is bioremediation, that is the utilization of POP-degrading microbes. Especially useful can be non-ligninolytic fungi, as their fast-growing mycelia can reach POP molecules strongly bond to soil minerals or humus fraction inaccessible to bacteria. The mobilized POP molecules are incorporated into the fungal plasma membrane where their degradation begins. The presence of POP molecules in the membranes can change their physical properties and trigger toxic effects to the cell. To avoid these phenomena fungi can quickly remodel the phospholipid composition of their membrane with employing different phospholipases and acyltransferases. However, if the presence of POP downregulates the phospholipases, toxic effects and the final death of microbial cells are highly probable. In our studies we applied multicomponent Langmuir monolayers with their composition mimicking fungal plasma membranes and studied their interactions with two different microbial phospholipases: phospholipase C (α-toxin) and phospholipase A1 (*Lecitase ultra*). The model membranes were doped with selected POPs that are frequently found in contaminated soils. It turned out that most of the employed POPs do not downregulate considerably the activity of phospholipases, which is a good prognostics for the application of non-ligninolytic fungi in bioremediation.

1. Introduction

Soils are the final sink for multiple organic pollutants emitted to the environment by anthropogenic activity [1,2]. Most of these molecules are rapidly mineralized by consortia of microbial decomposers, but some classified as persistent organic pollutants (POP) can remain unchanged in soils for years. [3,4]. POPs are persistent in the environment, biomagnify in trophic chains, are toxic and can be transported via the atmosphere on large distances from the emission source [5–7]. Finally, with rain or by dry deposition of airborne particles, they achieve soils, where they strongly bind to the organic humic matter [8]. The only economically possible means of remediation of large areas polluted with POPs is bioremediation [9,10]. POPs can be extracted from soils by plants using the phytoremediation method [11]; however, the most efficient seems to be the degradation performed by soil bacteria and fungi [9]. The POP-degrading soil consortia can be supported by the addition of nutrients to the soils, such as mineral fertilizers for bacteria or wood wastes for ligninolytic fungi. On the other hand, in the technique of bioaugmentation, the indigenous consortia can be broadened by inoculation of POP-degrading microbial species into the soils [12–14]. To metabolize the highly hydrophobic POP molecules, microorganisms first have to mobilize them and desorb from the mineral or humic matter. To achieve these goals, bacteria frequently release biosurfactants into their surrounding and absorb the POP molecules as solubilizates in biosurfactant micelles [15,16], whereas, the growing fungal mycelia can come in direct contact with the adsorbed POP molecules [17]. At the first stage of the microbial metabolism, POP molecules are transported via the cellular wall and incorporated into the plasma membrane [18,19]. In the hydrophobic environment of the membranes the first stages of the POP metabolism take place. The incorporation of POP molecules into the membrane can significantly change its structure, affect its permeability and fluidity which can lead to the occurrence of toxic effects of the POP presence and possible death of the microorganism cell [20–22]. To avoid this situation, soil

* Corresponding author.
E-mail address: broniato@chemia.uj.edu.pl (M. Broniatowski).

https://doi.org/10.1016/j.bbamem.2022.184018
Received 13 April 2022; Received in revised form 26 July 2022; Accepted 28 July 2022
Available online 1 August 2022

microorganisms exposed to hydrophobic toxins modify the phospholipid composition of their membranes [23,24]. To achieve this goal, that is to remodel the phospholipid matrix, different phospholipases are applied [25–27]. Phospholipases from the A1, A2 or B families can detach the fatty acyl chain in the *sn*-1, *sn*-2 or both positions of the glycerol backbone, respectively [28]. On the other hand, phospholipase C can cut the whole phosphate group from phosphatidylglycerol leading to the formation of diacylglycerol [29]. These reactions can be considered as the degradation of the membrane, but are also the first step of the phospholipid replacement. The cleaved fatty acid chain can be exchanged from shorter to longer or from unsaturated to saturated and a new different headgroup can be joined to the diacylglycerol molecule [30]. The activity of microbial phospholipases is directly related to the possibility of fast membrane reshaping and adaptation to changing external conditions. However, the effects of the presence of POP molecules in the microbial plasma membrane on its resistance/susceptibility to the action of phospholipases have not been investigated.

To shed light on these phenomena we employed Langmuir monolayers mimicking with their composition fungal plasma membranes and studied the effects of the incorporation of POP molecules on their physical properties and their interactions with microbial phospholipase C and phospholipase A1. In our studies, we applied selected POP molecules causing severe contamination of arable soils, representatives of polycyclic aromatic hydrocarbons (PAH), polychlorinated cyclodiene pesticides (CP), and polychlorinated biphenyls (PCB). Benzo[*a*]pyrene (BAP) was applied as a representative of PAHs, endosulfan (EDS) of CP and 4,4′-dichlorobiphenyl (PCB 15) and 3,3′,5,5′-tetrachlorobiphenyl (PCB 52) as representatives of PCB. These four selected POP representatives are significant soil contaminants, can be toxic to microorganisms [31], and were proved in our previous research to be especially membrane-active as compared to other congeners or similar compounds belonging to the same POP classes [32–34]. The employment of these four representative POP molecules guarantees their incorporation into the model membranes, which enables the discussion of the effects of the presence of POP within the membrane on its interactions with phospholipases. Two different microbial phospholipases were applied in the studies *Clostridium perfringens* α-toxin [35], that is an enzyme of PLC activity and *Lecitase ultra* – a fungal hybrid enzyme of PLA1 activity [36]. These two enzymes belong to the vast class of phospholipases, but differ profoundly in their structure, origin, and mode of action. These differences enable discussion of the general versus specific effects exerted on membrane-remodeling enzymes by the presence of POP molecules incorporated into the model membrane. The model membranes were characterized by mutually complementary mechanic, microscopic, and X-ray diffraction methods. Namely, the surface pressure (π) – mean molecular area (A) isotherms were recorded upon the monolayer compression and mean molecular area (A) – time (t) curves were measured in the penetration experiments after the enzyme solution injection into the aqueous subphase. The morphology of the model membranes was monitored by Brewster angle microscopy (BAM) and the interactions of the membrane lipids with POP molecules were studied at the molecular level with the application of Grazing incidence X-ray diffraction.

2. Experimental

2.1. Materials

Phospholipids employed in the studies: 1,2-dimyristoyl-*sn*-glycero-3-phosphocholine (DMPC), 1-palmitoyl-2-oleoyl-*sn*-glycero-3-phosphocholine (POPC), 1,2-dipalmitoyl-*sn*-glycero-3-phosphoethanolamine (DPPE), 1-palmitoyl-2-oleoyl-*sn*-glycero-3-phosphoethanolamine (POPE) and ergosterol were purchased from Avanti Polar Lipids. All these lipids were lyophilized powdered samples, which were stored at −20 °C. The enzymes: phospholipase C from *Clostridium perfringens*, phospholipase A1 expressed in *Aspergillus oryzae* (*L. ultra*) and lipase from *Chromobacterium viscosum* were purchased from Sigma Aldrich. The solvents applied in the studies, chloroform (99.9 % HPLC grade, stabilized by ethanol) and methanol (99.9 %, HPLC grade) were bought from Merck Sigma Aldrich. The components of the buffers: N-(2-hydroxyethyl)piperazine-N′-(2-ethanesulfonic acid) (HEPES, 99.5 %), citric acid (99.5 %), sodium chloride (99.5 %), calcium chloride (99.5 %) and zinc nitrate hexahydrate (99 %) were also purchased from Merck Sigma Aldrich. Ultrapure water of 18.2 MΩ·cm was produced in the laboratory with the use of Merck Millipore water purification unit (Synergy 12). The studied persistent organic pollutants: benzo[*a*]pyrene (BAP), endosulfan (EDS), PCB 15 (4,4′-dichlorobiphenyl) and PCB 52 (2,2′,5,5′-tetrachlorobiphenyl) were purchased from Merck Sigma-Aldrich as analytical standards of the purity ≥99 %. Structural formulae of the studied POPs are shown in Scheme 1.

2.2. Preparation of lipids and enzymes

Samples of the lipids were weighted on a Mettler Toledo balance with the accuracy of 10 μg and dissolved in chloroform/methanol 9/1 v/v mixture. The concentrations of the solutions applied for Langmuir monolayer formation were ca. 0.25 mg/mL (ca. $3.5 \cdot 10^{-4}$ M depending on the phospholipid and ca. $6.3 \cdot 10^{-4}$ M for ergosterol). Multicomponent solutions were prepared in glass vials just before the experiments by mixing the appropriate volumes of the stock solutions.

The sample of PLC (125 u/sample, 1u liberates 1 μmol of water soluble organic phosphorus from egg yolk L-α-phosphatidylcholine in 1 min at pH 7.3 at 37 °C) was dissolved in HEPES buffer in a 25 mL volumetric flask. The composition of the buffer was as follows: 0.001 mol of HEPES, 0.15 mol of NaCl, 0.005 mol of $CaCl_2$ and 0.0005 mol of $Zn(NO_3)_2{\cdot}6H_2O$. 1 M NaOH was added to the solution to achieve the pH of 7.3 [37]. The solution was divided onto 0.5 mL aliquots to glass vials and refrigerated at −20 °C. For a typical experiment on the Langmuir trough 100 μL of this PLC solution was injected via the injection port to the subphase leading finally to the concentration of 0.002 u/mL.

Lipase from *C. viscosum* (100 ku/sample, where 1u is defined as the amount of enzyme that will release 1.0 μmol of fatty acids from olive oil per min at 37 °C, pH 8.0) was added directly to the subphase (HEPES). 4 mg (10 ku) of this enzyme was dissolved in a 10 mL volumetric flask in HEPES. This solution was divided onto 0.5 mL aliquots and refrigerated. One aliquot was added to one dm^3 of the HEPES subphase.

L. ultra expressed in *A. oryzae* was bought from Sigma Aldrich as an aqueous solution of the activity ≥10 ku/g. The sample was stored at 2 °C. Fresh solutions of this enzyme were prepared just before the experiments: 21 μL (25 mg, 250 u) of this formulation was transferred to a 10 mL volumetric flask and dissolved in citric buffer (pH 6.5) of the concentration of 0.01 M. In a typical experiment 200 μL of this solution was injected into the subphase leading to the activity of the enzyme of 0.02 u/mL.

2.3. Subphases

All the experiments with PLC were performed on the HEPES buffer of the above mentioned composition containing the lipase from *C. viscosum* of the activity of 0.5 u/mL. The lipase was added to the subphase to perform the further degradation of the diacylglycerols formed in the reaction of PLC with membrane phospholipids enabling the desorption of the lysolipids from the air/water interface. The activity of PLC is monitored by the evolution of the mean molecular area over time. The formation of water soluble products leads to a decrease of A during the reaction, which facilitates monitoring of the progress of the enzymatic reaction and estimation of its apparent rate. The presence of water insoluble diacylglycerols at the air-water interface would mask the effects of the PLC activity.

The experiments with PLA1 were performed on citric buffer of 0.01 M concentration and pH of 6.5.

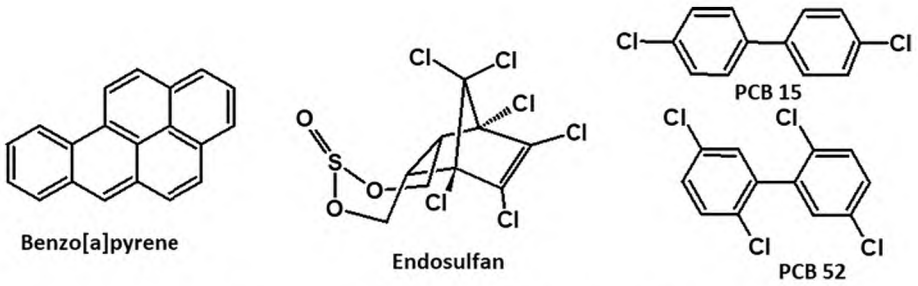

Scheme 1. Structural formulae of the studied POPs.

2.4. Techniques

2.4.1. Langmuir monolayer studies

Three Langmuir troughs were employed in the studies: a double barrier KSV-NIMA (Biolin Scientific, Sweden) trough of total area of 273 cm^2 was used for the routine π-A isotherm registration, a larger double barrier KSV-NIMA trough of total area of 580 cm^2 was used in the BAM experiments, whereas in the SOLEIL Synchrotron at the Sirius beamline a custom R&K single barrier trough of an approximate area of 500 cm^2 was installed. After an experiment, the monolayer material was disposed from the surface with a vacuum aspirator and then the subphase was removed. The troughs were wiped first with a tissue soaked in chloroform then with isopropanol and rinsed with plentiful of ultrapure water. The troughs were filled with the proper subphase and the appropriate volume of lipid chloroform solution was deposited at the subphase/air interface with the application of Hamilton analytical syringes. The troughs were left for 10 min for chloroform evaporation, then the monolayers were compressed at compression rate of 10 mm·min^{-1}. Surface pressure π was monitored with a Wilhelmy-plate electrobalance (KSV NIMA) with a rectangular plate of filtration paper (Whatman, ashless) applied as surface pressure sensor, with the uncertainty of ±0.05 mN/m. The π-A isotherms were measured at least three times and the uncertainty of the mean molecular area A was ±1 $Å^2$/molecule. The temperature of the subphase was controlled by a water-circulating bath. All the experiments were performed at 20 ± 0.1 °C.

Compression modulus C_S^{-1} was calculated from the course of π-A isotherms according to its definition [38]: $C_S^{-1} = -A\left(\frac{\partial\pi}{\partial A}\right)_{T,p,n}$, where the indices T,p,n refer to the: temperature of the measurement, external pressure and composition of the monolayer.

For the ternary monolayers composed of phosphatidylcholines, phosphatidylethanolamines and ergosterol differing in mole ratio of ergosterol thermodynamic analysis of the two-dimensional functions of mixing was performed. For these systems the excess free energy of mixing ΔG^{exc} was calculated. This function is defined as follows [39]:

$$\Delta G^{exc} = N_A \int_0^{\pi} A^{exc} d\pi$$

where N_A – Avogadro number, A^{exc} – excess area of mixing.

$$A^{exc} = A - A_{id},$$

where A is the mean molecular area observed at a given π value for the ternary monolayer, and A_{id} is the area calculated for ideal mixing as a weighted average:

$$A_{id} = A_1X_1 + A_2X_2 + A_3X_3,$$

where A_1, A_2 and A_3 are the mean molecular areas observed at the same π value for one-component monolayers of substances 1, 2 and 3 and X_1, X_2 and X_3 are mole ratios of substances 1, 2 and 3 in the studied monolayer.

2.4.2. Experiments with the phospholipases

In a typical experiment regarding the activity of the studied enzymes toward a given model membrane the monolayer was compressed to the surface pressure of 20 mN/m. Then the surface pressure was kept constant at this value and 20 min was left for the monolayer stabilization. Then appropriate volume of the studied enzyme was injected via an injection port into the subphase (into the well of the Langmuir-Blodgett trough). The subphase in the well was stirred by a magnetic stirrer to facilitate the even distribution of the injected enzyme. In such an experiment temporal evolution of the mean molecular area (A-t curve) at constant surface pressure was registered.

When a phospholipase interacts with model membranes (Langmuir monolayers at the air/solution interface, liposomes in the solution) the kinetics of the enzymatic reaction follows usually the lag-burst mechanism [40,41]. At the beginning of the experiment after the injection of the enzyme solution into the subphase the phospholipase distributes in the subphase, adsorbs to the model membrane and starts the degradation of the first phospholipid molecules. The response of the model system, measured here by the change of the mean molecular area, is slow. However, the generation of first lysolipid molecule induces the formation of membrane defects and accelerates significantly the reaction, so the response of the model system is fast [42]. Finally, due to the extinction of the substrates preferred by the studied enzyme, membrane reorganization and possible enzyme inhibition the reaction slows down. Typically the time-response curve (here A-t) measured in such an experiment has a sigmoidal course. The middle part of the sigmoid has an approximately linear character. Fitting tangent lines to the first section of the sigmoid (lag phase), the linear part of the sigmoid (burst phase) and the final section of the sigmoid (slow, asymptotic change of the measured response of the system) enables the estimation of the beginning and end of the burst phase. The slope of the linear part of the A-t curve, *s* can be employed as an estimation of the rate of the enzymatic reaction [37,43]. In our experiments all the A-t curves were measured at least 3 times. Straight lines were fit by linear regression to the linear part of the A-t curve, which enabled the estimation of the average *s* value and its standard deviation. All the measured A-t curves, lag time (t_1) and end of the burst phase (t_2), *s* coefficients and R factors of the linear regression can be found in Supporting Materials.

2.4.3. Brewster angle microscopy

UltraBAM instrument (Accurion GmbH, Goettingen, Germany) equipped with a 50 mW laser emitting p-polarized light at a wavelength of 658 nm, a 10× magnification objective, polarizer, analyzer and a CCD camera was used. The spatial resolution of the microscope was 2 μm. The foregoing apparatus and the Langmuir trough were placed on a table (Standa Ltd., Vilnius, Lithuania) equipped with active vibration isolation system (antivibration system VarioBasic 40, Halcyonics, Göttingen, Germany).

2.4.4. Grazing incidence X-ray diffraction

The experiments were performed at the SIRIUS beamline in SOLEIL synchrotron (Gif-sur-Yvette, France) using the dedicated liquid surface diffractometer. The Langmuir trough (R&K GmBh electronics, Germany)

was mounted on the goniometer in a gas tight box with Kapton windows. The applied energy of the X-ray beam (7.92 keV, $\lambda = 1.565$ Å) is high which can result in serious beam damage to the investigated monolayer. To avoid these phenomena, the experimental chamber was sealed and carefully flashed with helium to reduce the oxygen level to values lower than 1 %, as most of the beam damages are related to the generation of reactive oxygen species and the oxidation of the phospholipid molecules. Then the monolayer was compressed to the target surface pressure of 20 mN/m, which afterward was held constant during the entire experiment. The detailed construction of the diffractometer working at the SIRIUS beamline and the parameters of the synchrotron beam applied in the GIXD experiments are described on the SOLEIL web site (www.synchrotron-soleil.fr). The scattered signal was detected using a Pilatus3 2D pixel detector (Dectris Ltd., Switzerland). This detector is used as 1D detector through the combined use of a Soller slits collimator oriented vertically to fix the in-plane 2θ resolution and an integration of the 2D image horizontally to obtain a 1D spectrum. The achieved resolution was about 0.002 $Å^{-1}$. The spectra were obtained by scanning the in-plane 2θ angle. At each point, the vertically scattered intensity was recorded to obtain finally the intensity map $I(Q_{xy},Q_z)$, where Q_{xy} is the scattering vector component in the monolayer plane, and Q_z is the vertical component along the z-axis. The $I(Q_{xy},Q_z)$ diffractograms were integrated along the vertical distribution of Q_z to obtain the Bragg peaks $I(Q_{xy})$. The estimation of the full width at half maximum (FWHM) of Bragg peak enables the calculation of the L_{xy} parameter, which is related to the range of 2D crystallinity, $L_{xy} \approx 0.88 \cdot 2\pi/FWHM_{peak}$. Further details of this technique can be found in the introductory papers by Kjaer [44] an Als Nielsen and co-authors [45]. All the GIXD experiments were performed on monolayers compressed to 20 mN/m. This is a value lower than 30 mN/m usually accepted as a pressure at which the packing of acyl chains in the monolayer is comparable to that in the bilayer. However, both at 20 and at 30 mN/m the π-A isotherm of M2 was very steep, with approximately the same slope, and the corresponding C_S^{-1} values in both cases suggest liquid condensed state of the monolayer. Also BAM images depicted practically identical morphology of the M2 monolayer both at 20 and at 30 mN/m. For the GIXD experiment the monolayer is compressed to the required surface pressure and kept in that condition for about one hour. Therefore, we avoided the pressure of 30 mN/m as at that conditions 3D lipid aggregates frequently evolve from the Langmuir monolayers, which then slowly collapse with time.

3. Results and discussion

3.1. Optimization of the models of fungal plasma membranes

Fungal plasma membranes are generally reach in phosphatidylcholines (PC) and phosphatidylethanolamines (PE) [46–50], whereas the next important components are phosphatidylserines and phosphatidylinositols, the content of which depends strongly on the fungal species [50]. Similarly to animal and contrary to bacterial membranes, phosphatidylglycerols and cardiolipins are not present in the fungal plasma membranes but can be found in the mitochondrial membranes. In first approximation, the molar fraction of PC/PE in fungal plasma membranes is 1/1, and this proportion was acquired in our studies. Based on multiple studies on the distribution of the fatty acid chains within the phospholipid molecules in fungal plasma membranes, it can be stated that statistically the acyl chain in the *sn*-1 position of the glycerol backbone is saturated, whereas that in the *sn*-2 position *cis*-unsaturated [47,51]. Taking also into account the most frequent lengths of the chains very often the 1-palmitoyl-2-oleoyl-*sn*-glycero-3-phospholipids are applied for the modeling of microbial membranes [52].

In the present studies, two models of fungal membranes were proposed, the first M1 based on the POPC/POPE mixture and the M2 model in which saturated phospholipids DMPC and DPPE were applied. Indeed, reacting to environmental stimuli, such as increased contamination, salinity or temperature, microbes frequently remodel their membrane phospholipids changing the unsaturated fatty acids by saturated [47,53,54]. The application of the saturated phospholipids enabled the effective application of Brewster angle microscopy and X-ray diffraction in our studies, as these methods cannot be applied for liquid-expanded monolayers formed of unsaturated lipids. DMPC was used, as it is effectively digested by PLC and PLA1, whereas for DPPC or DSPC the rates of the enzymatic hydrolysis were much lower [37]. A crucial role in fungal membranes plays ergosterol, which is the most widespread lipid in fungal membranes [55,56]. The mole fraction of ergosterol to phospholipid depends on the particular fungal species and environmental conditions to which it is exposed. Some authors claimed that the ergosterol/phospholipid fraction can achieve even the value of 3 but the value of 1 meaning comparable amount of ergosterol and phospholipid molecules in the fungal membrane is more reliable; however, this value can also be lower than 1 [57]. Ergosterol is not evenly distributed in the membrane being more abundant in the inner cytoplasmic leaflet and in lipid rafts [58,59]. Moreover, the amount of ergosterol can be considerably increased when fungi are exposed to environmental toxicants [60].

Therefore, at the beginning of our research we have studied type M1 monolayers, that is these composed of POPC mixed with POPE in the statistically most typical 1/1 fraction, differing in the mole fraction of ergosterol with the aim of optimizing the composition of ternary lipid monolayers mimicking fungal plasma membranes. The data obtained in these experiments are presented in Fig. 1.

The POPC/POPE 1/1 monolayer has an expanded character and till its collapse remains in the liquid expanded (LE) state as the values of C_S^{-1} do not exceed 100 mN/m considered as the lower limit of the liquid condensed (LC) state of a Langmuir monolayer [38]. The addition of 10 mol% of ergosterol does not significantly affect the monolayer characteristics. No condensation effect is observed, at lower surface pressure values the π-A isotherm overlaps with that recorded for the undoped monolayer, while at higher surface pressures it is shifted to greater mean molecular areas. The C_S^{-1}-π curves at X(ergo) = 0 and X(ergo) = 0.1 overlap in the entire compression range. The increase of ergosterol content to X(ergo) = 0.3 leads to the shift of the isotherm to lower mean molecular areas, but the monolayer is still in the liquid expanded state and the C_S^{-1}-π curve overlaps with those recorded at X(ergo) = 0.1 and 0. Significant differences were observed at X(ergo) = 0.5. Upon the monolayer compression surface pressure starts to rise at ca. 65 $Å^2$/mol., that is at the same value as at X(ergo) = 0.3, but the increase of π is slower and a kind of a plateau can be noticed in the course of the π-A isotherm. After that, π rises much faster and the final section of the isotherm is very steep. This results in a completely different course of the C_S^{-1}-π curve which achieves the value of 100 mN/m at π = 15 mN/m and the maximal value of 220 mN/m at π = 33 mN/m. Thus, a strong condensing effect is observed at X(ergo) = 0.5 and the shallow plateau in the π-A isotherm observed at the beginning of the monolayer compression is the manifestation of the LE-LC phase transition taking place in that model membrane.

The excess free energy of mixing ΔG^{exc} was calculated for these monolayers (Fig. 1c). For all the investigated X(ergo), and all π values at which this function was calculated, ΔG^{exc} has a negative sign proving the energetically beneficial interactions between the phospholipid and ergosterol molecules in the investigated model membranes. The absolute values of ΔG^{exc} at X(ergo) = 0.3 and 0.5 are comparable, whereas at X(ergo) = 0.1 are two times lower.

The monolayers of the discussed series were compressed to π = 20 mN/m, and stabilized for 20 min at this surface pressure. Then the appropriate amount of PLC solution was injected into the subphase and the evolution of the mean molecular area was monitored. The resulting A-t curves are presented in Fig. 1d. All the A-t curves have a sigmoidal course typical to the kinetics of phospholipase catalyzed monolayer degradation. In the same experimental conditions *s* for POPE was reported to be −0.41 and for POPC – 0.90 ($Å^2 \cdot mol.^{-1} \cdot min^{-1}$) [37]. Here, for the 1/1 mixture of these phospholipids *s* is only −0.25, so it is a

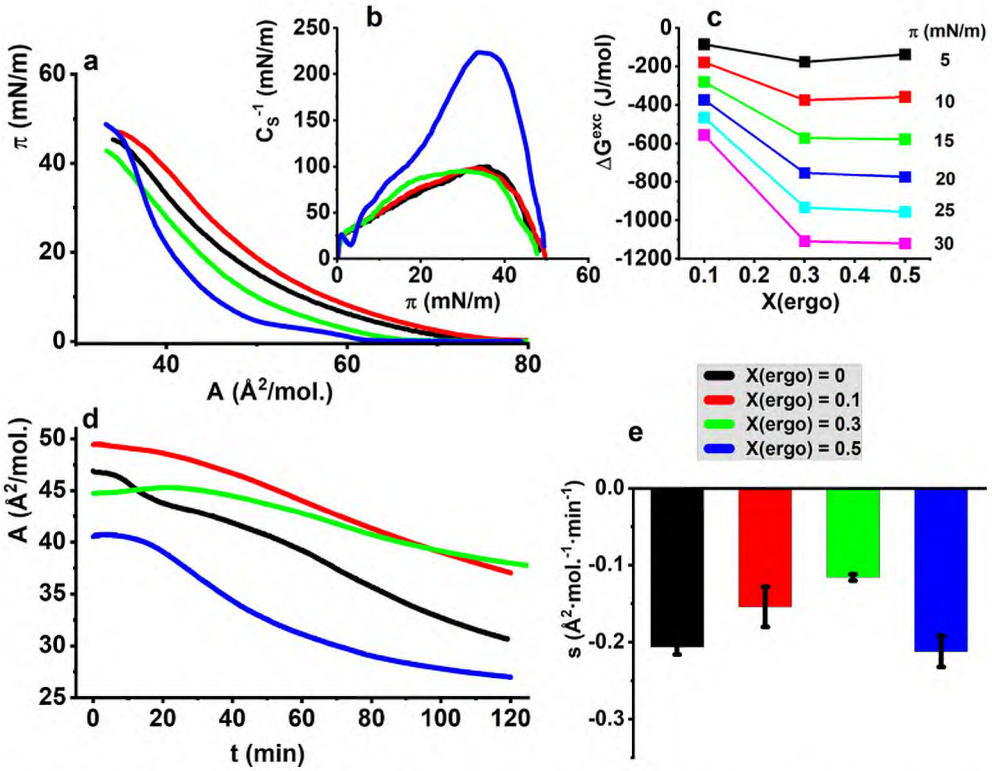

Fig. 1. Characterization of the POPC/POPE 1/1 membranes differing in the ergosterol fraction. a) π-A isotherms, b) C_S^{-1}-π dependences, c) ΔG^{exc}-X(ergo) plots, d) A-t curves registered after PLC injection, e) comparison of the *s* coefficients, the error bars are standard deviations of the *s* value.

remarkable example of the fact that the formation of model membranes of phospholipids belonging to different classes renders them more resistant to enzymatic degradation.

The introduction of ergosterol into the model membrane leads to a further reduction of *s* absolute value to 0.16 (Å^2·mol.$^{-1}$·min^{-1}) at X (ergo) = 0.1, and 0.11 (Å^2·mol.$^{-1}$·min^{-1}) at X(ergo) = 0.3. However, the further increase of X(ergo) to 0.5 causes the rise of *s* absolute value to 0.20 (Å^2·mol.$^{-1}$·min^{-1}).

As it was already mentioned the proportion of ergosterol in fungal membranes can change in a vast range, therefore, at the beginning of the studies we were looking for the most reliable model of the fungal plasma membrane. X(ergo) = 0.1 is in the light of the scientific literature rather to low. On the other hand, at X(ergo) = 0.5 the monolayers were too condensed and too stiff to reliably mimic the plasma membranes. Moreover, at this proportion phase separation and generation of membrane defects was highly probable. In such a case the texture of the membrane could be unrepeatable in subsequent experiments, which could negatively affect the reproducibility of the experiments with phospholipases. Therefore, the monolayers with X(ergo) = 0.3 seem most suitable for application as model fungal membranes. These membranes were acceptably fluid and simultaneously exhibited increased resistance to the action of phospholipases. The increased resistance of the membrane is beneficial for the experiments.

Regarding mechanical parameters, this monolayer was comparable to these at X(ergo) = 0 and 0.1, whereas when ΔG^{exc} is concerned, it was similar to that at X(ergo) = 0.5. Therefore, the ternary Langmuir monolayer containing 35 mol% of POPC, 35 mol% of POPE and 30 mol% of ergosterol was considered the most convenient model of the fungal plasma membrane for the further studies in this project. It was coded M1, whereas in the M2 model applied in the BAM and GIXD experiments saturated phospholipids DMPC and DPPE were applied (M2: 35 mol% of DMPC, 35 mol% of DPPE and 30 mol% of ergosterol).

In the further experiments the models M1 and M2 of fungal plasma membranes were doped in 10 mol% of the investigated POP molecules. These monolayers were compressed and the resultant π-A isotherms and C_S^{-1}-π curves are presented in Fig. 2.

It should be underlined that according to their definition POPs are highly hydrophobic and water insoluble. Indeed according to the literature the logarithms of the octanol/water partition coefficients pK_{OW} are: 6.08 for benzo[*a*]pyrene [61], 4.9 for endosulfan [62], 6.1 for PCB 52 [62] and 4.97 for PCB 15 [63]. Thus all the studied here POPs can be treated as completely water insoluble, which is important for the further interpretation of the experimental results. Neither of the four investigated POP molecules is surface active nor forms Langmuir monolayers. On the other hand, it was proved that these POPs can efficiently incorporate to model microbial membranes [32–34]. Their incorporation means the increase of the total number of molecules present at the air/subphase interface, so the π-A isotherm in first approximation should shift toward greater mean molecular area. However, such an effect was not observed for the M1 type model membranes doped with the investigated POPs. For the monolayers doped with PCB 15 and PCB 52 the π-A isotherms overlap with that measured for the undoped M1 monolayer, whereas for those doped with EDS and BAP the isotherms are shifted toward smaller mean molecular areas. However, at high surface pressure values, at 30 mN/m and above, the curves approach each other. These measured for the membrane doped with PCB 15 and PCB 52 are shifted toward greater mean molecular areas, whereas these for the monolayers doped with EDS and BAP overlap with the isotherm recorded for the undoped M1 monolayer. These observations mean that all the investigated POP molecules exert a condensing effect on the M1 membrane when incorporated into it. This effect is comparable for both the PCB congeners and is much more pronounced for EDS and BAP. Indeed, the condensing effect of the employed POP molecules is reflected in the values of compression modulus. The addition of the PCB congeners increases the maximal value of C_S^{-1} from 95 to 120 mN/m, the addition of EDS to 130 mN/m, whereas in the presence of BAP the maximal C_S^{-1} value was 155 mN/m.

The exchange of phospholipids in model fungal membranes with

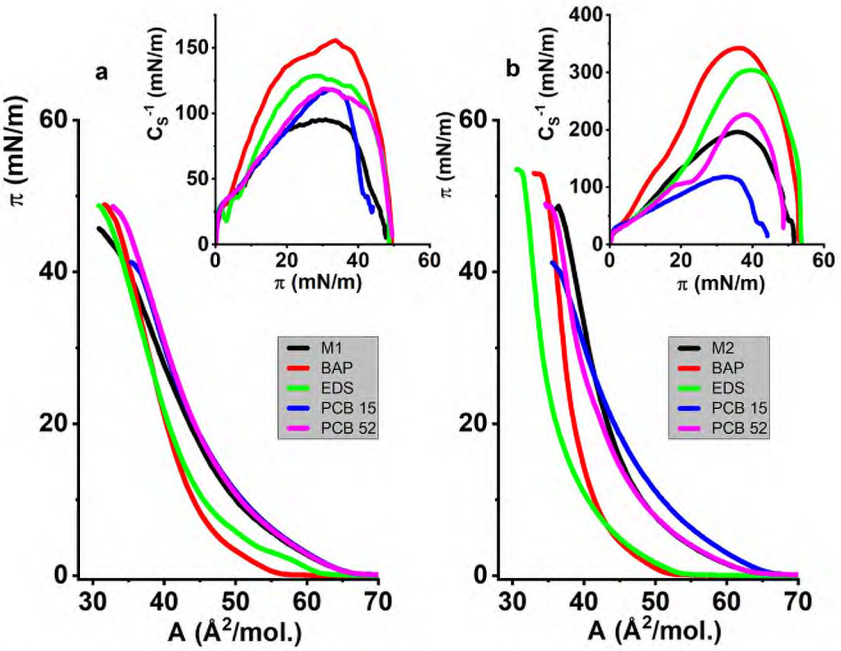

Fig. 2. π-A isotherms and C_S^{-1}-π curves for a) M1 and b) M2 model fungal membranes doped with the studied POPs.

their saturated counterparts leads to further differentiation over the employed pollutants. EDS and BAP still exert the condensing effect, but now it is much more pronounced. The presence of EDS increases the maximal value of compression modulus for the M2 model from 195 mN/m to 310 mN/m, whereas in the presence of BAP this value is even higher, 345 mN/m. Thus, it can be stated that when doped with 10 mol% of these POPs the state of the M2 model membrane is changed from liquid condensed to solid. The addition of PCB 52 only slightly affects the elasticity of the M2 monolayer, since the maximal C_S^{-1} is increased only to 230 mN/m. On the contrary, the addition of PCB 15 to the M2 model membrane leads to the lowering of the molecular order, expansion of the surface film, and a profound lowering of the maximal C_S^{-1} value to 117 mN/m.

The high values of C_S^{-1} observed for the undoped M2 model membrane and even higher values recorded when doped with EDS or BAP make periodic ordering of the monolayer-forming lipid molecules highly probable. Therefore, to verify the 2D crystallinity of these systems and to study the effects exerted on lipid ordering at the molecular scale, GIXD experiments were performed and the results obtained for the undoped M2 monolayer are presented in Fig. 3.

A strong diffraction signal was recorded for the M2 model membrane proving its 2D crystallinity. This signal is triply degenerate and splits in three signals of comparable intensity. One of them indexed ⟨−1,1⟩ with the h,k Muller indices has its intensity maximum at $Q_{xy} = 1.494$ Å^{-1} and Q_z close to 0 Å^{-1}, the second at $Q_{xy} = 1.472$ Å^{-1} and $Q_z = 0.38$ Å^{-1}, and the third at $Q_{xy} = 1.445$ Å^{-1} and $Q_z = 0.47$ Å^{-1}. Such a set of diffraction signals defines the oblique 2D crystal lattice. The lattice parameters a,b and γ, area A of the unit cell, tilt angle τ, and L_{xy} – the parameter measuring the 2D crystallinity range within the monolayer plane are collected in Table 1.

The addition of the studied POP molecules to the M2 model membrane does not practically change the structural parameters. In all the cases, the tilt angle τ changes in the narrow compartment between 18 and 19°. There are also no significant changes in the L_{xy} parameters. Thus, at first glance there is a contradiction between the data acquired in the Langmuir experiments (π-A isotherms, C_S^{-1}-π curves) and the GIXD results. The addition of BAP and EDS triggered a profound increase of the monolayer condensation, whereas PCB 15 leads to the monolayer expansion. No of these effects are visible in the GIXD results. Therefore, it can be assumed that two kinds of highly condensed domains are present at the air/water interface. The first-type domains are composed solely of the M2 membrane lipids and are 2D crystalline, whereas the second-type domains contain also the POP molecules and are amorphous. However, a question can be asked how it is possible, why POP

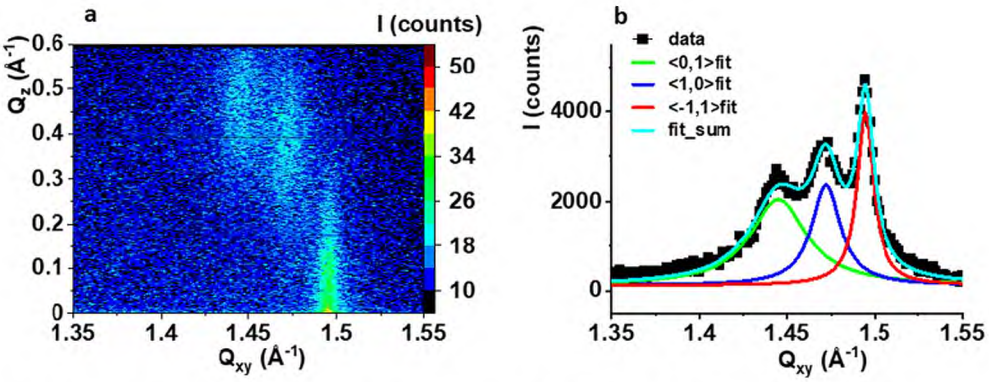

Fig. 3. GIXD results for the M2 model membrane. a) $I(Q_{xy},Q_z)$ intensity contour map, b) Bragg peak $I(Q_{xy})$ profiles. Solid lines are Lorentz curves fit to the experimental data.

Table 1
Parameters describing the 2D crystallinity extracted from the GIXD data.

System	a, b, γ (Å, Å, deg)	A (Å^2)	τ (deg)	L_{xy} (Å)
Model	4.852, 4.973, 118.4	21.10	19.0	$L_{\langle 0,1\rangle} = 142 \pm 7$ $L_{\langle 1,0\rangle} = 276 \pm 22$ $L_{\langle -1,1\rangle} = 477 \pm 20$
BAP	4.853, 4.937, 118.5	21.06	18.3	$L_{\langle 0,1\rangle} = 168 \pm 12$ $L_{\langle 1,0\rangle} = 276 \pm 31$ $L_{\langle -1,1\rangle} = 517 \pm 29$
EDS	4.855, 4.950, 118.3	21.15	18.9	$L_{\langle 0,1\rangle} = 173 \pm 11$ $L_{\langle 1,0\rangle} = 276 \pm 28$ $L_{\langle -1,1\rangle} = 489 \pm 22$
PCB 15	4.845, 4.926, 118.5	20.98	18.7	$L_{\langle 0,1\rangle} = 149 \pm 12$ $L_{\langle 1,0\rangle} = 325 \pm 38$ $L_{\langle -1,1\rangle} = 473 \pm 20$
PCB 52	4.851, 4.938, 118.4	21.08	19.1	$L_{\langle 0,1\rangle} = 276 \pm 14$ $L_{\langle 1,0\rangle} = 240 \pm 10$ $L_{\langle -1,1\rangle} = 521 \pm 20$

incorporate to some domains and the other remain undoped. This is probably related to the organization of the M2 monolayer. The 2D crystalline lattice is oblique and the signals are narrow, which results in large values of the L_{xy} parameters. On the other hand, for binary phospholipid-sterol domains, short ranges of 2D crystallinity were usually observed [64,65], so the GIXD signals were much wider than in the case discussed here. Therefore, it is probable that in the undoped M2 model membrane two types of condensed domains form. These enriched in ergosterol are amorphous, whereas these enriched in phospholipids are 2D crystalline. This situation reflects the phenomena observed in real fungal membranes where ergosterol-rich domains (lipid rafts) coexist with ergosterol-poor regions [59]. Therefore, it is highly probable that the studied POP molecules incorporate into the ergosterol enriched domains, leading to the observed changes in monolayer condensation. The postulated division of the M2 monolayer into amorphous and 2D crystalline domains can also be observed on the *meso* scale in the BAM images (Fig. 5) and will be discussed later.

The M1 and M2 membranes doped in the four investigated here POPs were compressed to 20 mN/m, stabilized under those conditions, and subjected to the action of PLC. The results: A-t curves and the comparisons of *s* coefficients are presented in Fig. 4.

It should be underlined that the A-t curves measured for the M1 and M2 models are similar regardless of differences in the saturation of the model-forming phospholipid molecules. Both the A-t curves are sigmoids, and the only differences can be noticed in the lag phase, since for the M1 membrane the lag time was 26 min, whereas for M2 it was 15 min. The *s* coefficients estimated from the course of the A-t curves in the burst phase are comparable, being ca. −0.1 (Å^2·mol.$^{-1}$·min^{-1}). In the presence of POPs the A-t curves are still sigmoids, but their courses can differ significantly from the curves registered for the undoped model membranes. The most noticeable was the effect of the presence of BAP in the M1 membrane, as the lag time increased to 40 min and the absolute value of *s* decreased from 0.105 to 0.028 (Å^2·mol.$^{-1}$·min^{-1}), that is 3.75 times. Thus, the presence of BAP significantly increases the resistance of the model fungal membrane to the PLC driven degradation. A similar effect was observed for the M2 model membrane, but the reduction of the absolute value of *s* was less drastic, since it changed from 0.097 to 0.052 (Å^2·mol.$^{-1}$·min^{-1}), that is 1.86 times. For M1 model membrane doped with the other three pollutants, only a slight reduction of *s* to ca. 0.08–0.09 (Å^2·mol.$^{-1}$·min^{-1}) was observed, so the presence of these POPs in the fungal membrane practically does not interfere with the activity of PLC. Different results were collected for the M2 membrane doped with these POPs. PCB 15 was the pollutant, the presence of which in the monolayer, lead to the most significant reduction of *s* absolute value from 0.097 to 0,031 (Å^2·mol.$^{-1}$·min^{-1}), that is 3.1 times. In addition, the presence of the second PCB congener leads to a profound reduction of *s* absolute value to 0.05 (Å^2·mol.$^{-1}$·min^{-1}). Only the presence of EDS in the M2 monolayer had no effect on the membrane susceptibility to PLC action. Thus, it is clearly visible that the structure of the membrane-forming lipids, and especially the saturation of the acyl chains is the crucial factor responsible for the monolayer resistance/susceptibility to PLC action after the incorporation of POPs. Phospholipases are most active on the boundaries of membrane domains [66,67], and the increase of the domain condensation usually lowers their activity and can even lead to complete inhibition [67]. As it was discussed for the M1 monolayer, the incorporation of BAP leads to a greater

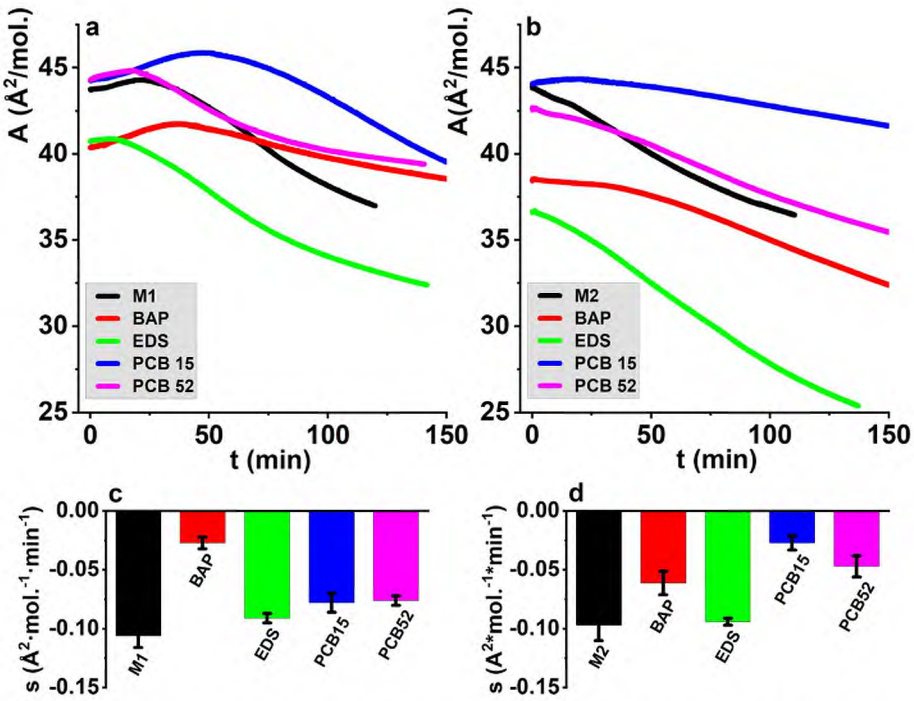

Fig. 4. Characteristics of the PLC interactions with the M1 and M2 model membranes doped with the investigated POPs. a,b) A-t curves, a) M1, b) M2, c,d) comparison of *s* coefficients c) M1, d) M2., error bars are standard deviations from the average *s* value.

increase in condensation than in the case of the other studied POPs. The significantly increased condensation of M1 membrane leads to the inhibition of PLC and to the significant reduction of the rate of the monitored enzymatic reaction. However, the observed phenomena cannot only be explained on the basis of the model membrane condensation. The addition of BAP and EDS to the M2 membrane lead to a similar, and very significant increase of monolayer condensation, expressed in the high C_S^{-1} values, but the effects on PLC activity were different. For the membrane doped in BAP the absolute value of *s* was twice reduced, but no effects were observed in the case of EDS.

To gain further insight into the interactions of the POP-doped model membranes with PLC the temporal evolution of the morphology of the M2-derived systems was observed with the application of Brewster angle microscopy and the resultant BAM images are gathered in Fig. 5.

The images collated in the first row of Fig. 5 are similar showing bright condensed domains on darker background. Typically, such images are interpreted as LC domains being in equilibrium with the LE continuum [68]. Thus, the *meso* scale images corroborate the idea inferred from the GIXD results that phospholipid-enriched 2D crystalline domains coexist with an amorphous ergosterol-enriched phase. It should also be underlined that the domains visible in the images in the first row of Fig. 5 are similar regardless of the presence of different POP molecules. They have an irregular shape and an approximate length of 10–15 μm. The lack of differences between the photos corroborates the conclusion drawn from the GIXD results that POP molecules are inserted into the ergosterol-rich amorphous phase. Regarding the temporal evolution of the undoped M2 model membrane, the image taken 60 min after the enzyme injection is comparable with that recorded at the beginning of the experiment. However, 120 min after the injection the image is completely different, since long fractal mutually fused domains are present in the photo. They are still in equilibrium with homogeneous, darker regions. Looking at Fig. 4b at the course of the A-t curve registered for M2 membrane, it can be noticed that 60 min after the enzyme injection the studied system is in the middle of the burst phase, whereas 120 min after the injection the curve flattens, which means the termination of the PLC catalyzed hydrolysis. As it was discussed in the literature [35,37], phosphatidylcholines are the preferred substrates for α-toxin, so the evolution of the domain morphology can be explained by the diminishing fraction of DMPC. The fractal domains observed 120 min after the enzyme injection might be formed only of DPPE. The temporal evolution of the morphology of the M2 monolayer doped with EDS and PCB 52 is similar to that observed for the pollutant-free M2 membrane. In contrast, the evolution of the texture of the M2 membrane doped with BAP and PCB 15 proceeds differently. For the monolayer containing BAP 60 min after the PLC injection the condensed domains are smaller and less numerous than at the beginning of the experiment. However, 120 min after the injection multiple condensed domains are again visible. They have different morphologies – are greater (length up to 30 μm), while their shape resembles snowflakes. The GIXD results proved that the investigated POP molecules did not incorporate into the 2D crystalline domains. Unfortunately, it is impossible to follow the evolution of the monolayer after the enzyme injection with the GIXD technique. As it was specified in the experimental, the Langmuir trough has to be sealed in a helium filled chamber during the experiment. Moreover, the R&K Langmuir trough installed in SOLEIL has not a well to which the enzyme solution could be injected. Therefore, it was impossible to check the crystal structure of the large domains visible in the image taken for BAP-doped M2 monolayer 120 min after the enzyme injection. It is a pity, because they have probably completely different composition than the domains observed at the beginning of the experiment. The slow hydrolysis of DMPC changes the composition of the domains and leads to the reduction of their size. On the other hand, BAP leads to profound condensation of the amorphous ergosterol-rich phase, so the DMPC molecules from this phase cannot be built into the 2D crystalline domains to compensate for these hydrolyzed. With time elapse, the composition of the system changes and probably BAP is included into the newly formed condensed domains. This idea is in accordance with the significant reduction of the darker areas of the homogeneous phase visible in the photo taken 120 min after the enzyme injection. Although PCB 15 disorganizes the model membrane and leads to its expansion, the evolution of the M2 monolayer doped with this pollutant was similar to that doped with BAP. Thus, probably in both cases new condensed domains containing the POP molecules form. Such POP-enriched domains are resistant to the PLC catalyzed hydrolysis.

To gain a more complex insight into the effects exerted by membrane incorporated POPs on phospholipase activity we applied *L. ultra* in our studies. *L. ultra* is a hybrid fungal enzyme of phospholipase A1 activity [36], which has a different structure and mode of action than the

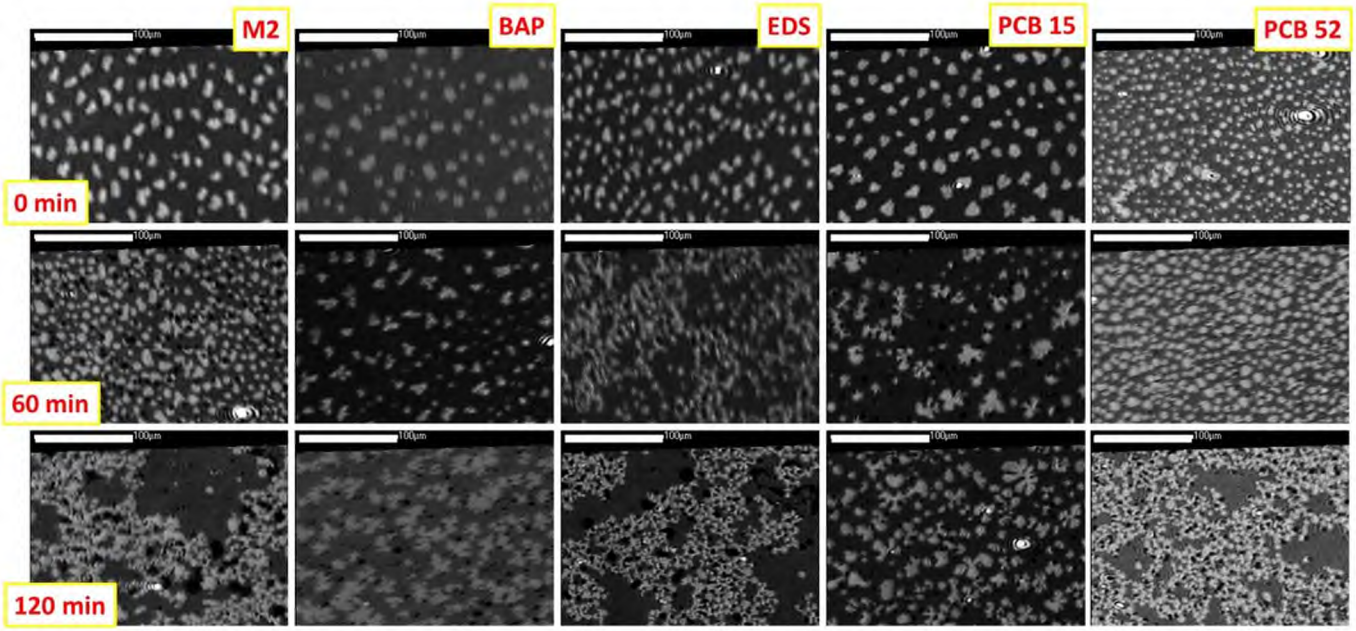

Fig. 5. Representative BAM images recorded for the M2 model membranes doped with 10 mol% of the investigated POPs. First row) images taken just after the PLC injection, second row) 60 min after the injection, third row) 120 min after the injection. The scale bar denotes 100 μm. All the images were taken at $\pi = 20$ mN/m.

bacterial PLC α-toxin. To work with this enzyme, we also changed the subphase from HEPES to 0.01 M citrate buffer of the pH of 6.5. The M1 and M2 model membranes pure and doped with the investigated POPs were formed on that subphase and compressed to 20 mN/m. After 20 min of stabilization, the PLA1 solution was injected into the subphase. The resultant A-t curves and the comparisons of the *s* coefficients are presented in Fig. 6.

Following the typical kinetics of the reaction of phospholipases with Langmuir monolayers, all the A-t curves in Fig. 6 are sigmoidal. There is an important difference between the M1 and M2 model, as the rate of M1 hydrolysis is 3 times higher than that of M2, which is reflected in the values of *s* coefficient, 0.31 and 0.12 ($Å^2 \cdot mol.^{-1} \cdot min^{-1}$), respectively. Regarding the M1 model membrane, the results are qualitatively similar to those presented in Fig. 4 where the interactions with PLC are discussed. Again the greatest reduction of the absolute value of *s* from 0.31 to 0.15 ($Å^2 \cdot mol.^{-1} \cdot min^{-1}$) was observed for the membrane doped with BAP. However, now a two-time reduction is observed, whereas in the experiments with PLC a four-time reduction was noticed. For the M1 monolayer doped with EDS no change of the *s* coefficient value was observed, whereas for the membranes doped with PCB 15 and PCB 52 moderate reduction of the absolute value of *s* was noticed. As it was already mentioned the results obtained for the M1 model membrane in the experiments with PLC and PLA1 were qualitatively comparable. In contrast, completely different results were obtained for the M2 model. The introduction of BAP into the M2 model membrane did not change the rate of the enzymatic reaction, as the *s* coefficients for the undoped monolayer and that enriched in BAP were identical within the limit of experimental error. For the M2 monolayers doped in the remaining three POP a slight reduction of the absolute value of *s* coefficient from 0.12 to 0.9–0.1 ($Å^2 \cdot mol.^{-1} \cdot min^{-1}$) was observed.

The temporal evolution of M2 model membranes subjected to the action of PLA1 was also visualized with the application of Brewster angle microscopy and the resultant representative images are presented in Fig. 7.

The morphology of the M2 monolayer spread on citrate buffer is the same as presented in Fig. 5 for the monolayer spread on HEPES, so the buffer applied as the subphase has no effect on the state of the monolayer and the evolution of the condensed domains. Consistently with the photos presented in the first row of Fig. 5, also here no significant effects of the addition of the investigated POPs on the domain morphology were noticed. 60 min after PLA1 injection, the condensed domains visible in the BAM image were approximately two times larger than at the beginning of the experiment, so it can be inferred that the composition of these domains was successively modified by the enzyme. 120 min after the injection, the domains further grew, no fractal domains similar to these observed in Fig. 5 were noticed. The differences between α-toxin and *Lecitase* may be mainly related their substrate preferences. α toxin prefers phosphatidylcholines over phosphatidylethanolamines, whereas for *Lecitase* this preference is not so pronounced [37,69]. With time elapse after *Lecitase* injection, the DMPC/DPPE ratio probably decreases, but even 120 min after the injection DMPC molecules are still present in the domains.

For the M2 monolayer enriched in BAP, the evolution of the morphology in time is virtually identical to that of the undoped monolayer. This is in accordance with the data inferred from the A-t curves, as the *s* coefficients were identical for these monolayers. *L. ultra* is not as vulnerable to the condensation of the monolayer as α-toxin [36,69], therefore, the increased condensation of the amorphous phase of the model membrane does not affect the activity of the enzyme. On the other hand, phospholipases act mainly on the boundaries of lipid domains [64]. The presence of BAP does not affect the domain morphology, which is a second reason explaining the identical interactions of the pure M2 membrane and that doped with BAP. In the presence of the other three POPs changes of the domain morphology can already be noticed 60 min after the enzyme injection. They are less noticeable for PCB 52, more progressed for EDS and are especially pronounced for the monolayer doped with PCB 15. It is probable that with time elapse and due to the changes in the domain phospholipid composition, some POP molecules are incorporated into these domains, lowering the rate of the enzymatic reaction. However, as can be seen in Fig. 6 d, this effect is not so pronounced as in the case of PLC (Fig. 4d).

4. Conclusions

There are multiple scientific reports regarding the effects of POP pollution on the activity of phospholipases [70–72]. However, these

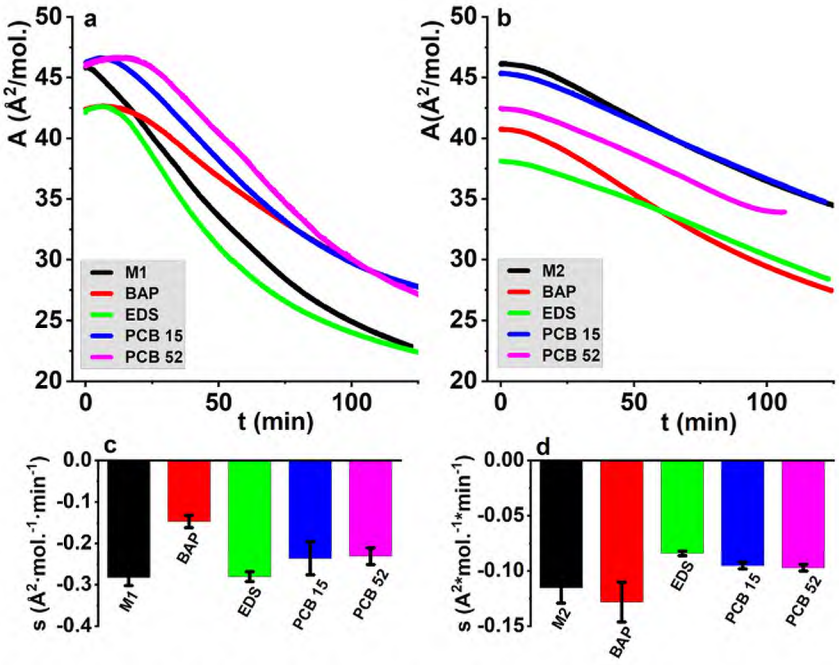

Fig. 6. Characteristics of the PLA1 interactions with the M1 and M2 model membranes doped with the investigated POPs. a,b) A-t curves, a) M1, b) M2, c,d) comparison of *s* coefficients c) M1, d) M2. Error bars are standard deviations of the average *s* value.

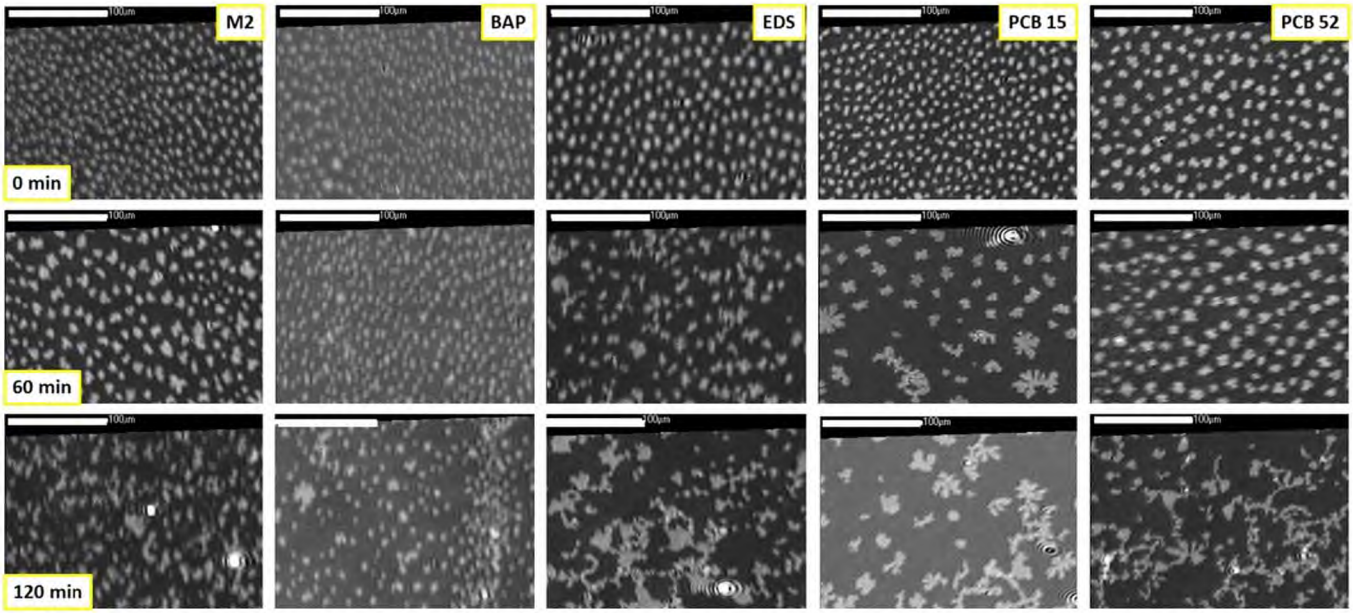

Fig. 7. Representative BAM images recorded for the M2 model membranes doped with 10 mol% of the investigated POPs. First row) images taken just after PLA1 injection, second row) 60 min after the injection, third row) 120 min after the injection. The scale bar denotes 100 μm. All the images were taken at $\pi = 20$ mN/m.

studies were performed mainly on animal cell lines and considered the expression of genes that encode phospholipases. The presence of selected POPs such as PAHs or PCBs can significantly affect the expression of phospholipases in animal cells and hence the composition of plasma membranes. On the other hand, there were no studies regarding the effects of the POP molecules incorporated into the membrane on the activity of phospholipases. Phospholipase driven remodeling of the microbial membrane can have crucial significance for the adaptation of a microorganism to harsh environmental conditions, such as the presence of pollutants, increased salinity, too-high or too-low temperature or nontypical pH [73–75]. To remediate soil contaminating POPs, microorganisms must first adsorb these hydrophobic molecules from the environment and incorporate them into their plasma membranes, where the biodegradation process begins. However, the membrane inserted POP molecules can interfere with the membrane function, change its fluidity and permeability, which can lead to the death of the microorganism and the impoverishment of the decomposer consortium. To avoid these phenomena fast remodeling of the membrane phospholipid composition can be necessary, which is achieved by the action of phospholipases and transacylases [73,76]. In our studies we applied Langmuir monolayers mimicking in their composition fungal plasma membranes, studied the effects of the presence of four selected POPs on the physical properties of these membranes and their interactions with two different phospholipases. The incorporation of the investigated POPs to M1 model membrane composed of unsaturated lipids weakly affected its interactions with both the studied phospholipases. For both the employed PCB congeners and the polychlorinated pesticide endosulfan only slight reduction of the enzymatic reaction rate was noticed. This is a positive prognostics for the bioremediation of the soils contaminated with these pollutants. The presence of PCB 15, PCB 52 and EDS in the fungal plasma membrane does not disturb the activity of phospholipases, so fast remodeling of the phospholipid content would be possible. On the contrary, benzo[*a*]pyrene significantly lowers the rate of the enzymatic reactions both in the experiments with PLC as well as with PLA1. This is probably connected with the large increase of monolayer condensation caused by the introduction of this pollutant into the lipid matrix. This observation proves, that there can be specific POPs present in soils the incorporation of which into the membrane adversely affects the activity of phospholipases. Such pollutants can be highly toxic to soil fungi which can increase their recalcitrance, which was really observed for some PAHs [31]. The change of the model-forming phospholipids to those with saturated acyl chains (model M2) differentiated the studied enzymes. For the more aggressive PLA2 (*L. ultra*), the results were similar to those obtained for the unsaturated M1 model. On the contrary, the introduction of POPs to the M2 membrane significantly lowered the activity of PLC. However, typically unsaturated and polyunsaturated acyl chains dominate in fungal plasma membranes [50], so the phenomena observed for the M2 model are less probable in the real conditions. Generally, our results prove that the incorporation of POPs into the fungal plasma membrane would rather not affect the phospholipase-driven remodeling of the phospholipid content. This is a very positive conclusion encouraging for the application of non-ligninolytic in the bioremediation of POP contaminated soils.

Declaration of competing interest

The authors declare that they have no known competing financial interests or personal relationships that could have appeared to influence the work reported in this paper.

Acknowledgements

This project was financed by the National Science Centre (No 2016/21/B/ST5/00245). We gratefully acknowledge SOLEIL for provision of synchrotron radiation facilities and we would like to thank Dr. Philippe Fontaine for assistance in using SIRIUS beamline.

Appendix A. Supplementary data

Supplementary data to this article can be found online at https://doi.org/10.1016/j.bbamem.2022.184018.

References

[1] H. Lu, C.H. Mo, H.M. Zhao, L. Xiang, A. Katsoyiannis, Y.W. Li, Q.Y. Cai, M. H. Wong, Soil contamination and sources of phthalates and its health risk in China: a review, Environ. Res. 164 (2018) 417–429.

[2] K.T. Semple, A.W.J. Morriss, G.I. Paton, Bioavailability of hydrophobic organic contaminants in soils: fundamental concepts and techniques for analysis, Eur. J. Soil Sci. 54 (2003) 809–818.

[3] H.I. Gomes, C. Dias-Ferreira, A.B. Ribeiro, Overview of in situ and ex situ remediation technologies for PCB-contaminated soils and sediments and obstacles for full-scale application, Sci. Total Environ. 445–446 (2013) 237–260.

[4] M. Gavrilescu, Fate of pesticides in the environment and its bioremediation, Eng. Life Sci. 5 (2005) 497–526.

[5] D. Mackay, L.S. McCarty, M. MacLeod, On the validity of classifying chemicals for persistence, bioaccumulation, toxicity, and potential for long-range transport, Environ. Toxicol. Chem. 20 (2001) 1491–1498.

[6] R. Lohmann, K. Breivik, J. Dachs, D. Muir, Global fate of POPs: current and future research directions, Environ. Pollut. 150 (2007) 150–165.

[7] K.C. Jones, Persistent organic pollutants (POPs) and related chemicals in the global environment: some personal reflections, Environ. Sci. Technol. 55 (2021) 9400–9412.

[8] M. Pandelova, B. Henkelmann, B.M. Bussian, K.W. Schramm, Results of the second national forest soil inventory in Germany - interpretation of level and stock profiles for PCDD/F and PCB in terms of vegetation and humus type, Sci. Total Environ. 610–611 (2018) 1–9.

[9] N. Gaur, K. Narasimhulu, Y. PydiSetty, Recent advances in the bio-remediation of persistent organic pollutants and its effect on environment, J. Clean. Prod. 198 (2018) 1602–1631.

[10] R. Jing, S. Fusi, B.V. Kjellerup, Remediation of polychlorinated biphenyls (PCBs) in contaminated soils and sediment: state of knowledge and perspectives, Front. Environ. Sci. 6 (2018) 79.

[11] S. Ouvrard, P. Leglize, J.L. Morel, P.A.H. Phytoremediation, Rhisodegradation or rhizoattenuation, Int. J. Phytoremed. 16 (2014) 46–61.

[12] C.C. Azubuike, C.B. Chikere, G.C. Okpokwasili, Bioremediation techniques–classification based on site of application: principles, advantages, limitations and prospects, World J. Microbiol. Biotechnol. 32 (2016) 180.

[13] T.J. Gentry, C. Rensing, I.L. Pepper, New approaches for bioaugmentation as a remediation technology, Crit. Rev. Environ. Sci. Technol. 34 (2004) 447–494.

[14] M. Tyagi, M.M.R. da Fonseca, C.C.C.R. de Carvalho, Bioaugmentation and biostimulation strategies to improve the effectiveness of bioremediation processes, Biodegredation 22 (2011) 231–241.

[15] A.A. Jimoh, B. Lin, Production and characterization of lipopeptide biosurfactant producing Paenibacillus sp. D9 and its biodegradation of diesel fuel, Int. J. Environ. Sci. Technol. 16 (2019) 4143–4158.

[16] E. Kaczorek, A. Pacholak, A. Zdarta, W. Smułek, in: The impact of biosurfactants on microbial cell properties leading to hydrocarbon bioavailability increase 2, 2018, p. 35.

[17] A. Reyes-Cesar, A.E. Absalon, F.J. Fernandez, J.M. Gonzalez, D.V. Cortes-Espinosa, Biodegradation of a mixture of PAHs by non-ligninolytic fungal strains isolated from crude oil-contaminated soil, World J. Microbiol. Biotechnol. 30 (2014) 999–1009.

[18] E. Marco-Urrea, I. Garcia-Romera, E. Aranda, Potential of non-ligninolytic fungi in bioremediation of chlorinated and polycyclic aromatic hydrocarbons, New Biotechnol. 32 (2015) 620–628.

[19] Y. Fujita, H. Matsuoka, K. Hirooka, Regulation of fatty acid metabolism in bacteria, Mol. Microbiol. 66 (2007) 829–839.

[20] J. Sikkema, J.A.M. de Bont, B. Poolman, Mechanism of membrane toxicity of hydrocarbons, Microbiol. Rev. 59 (1995) 201–222.

[21] G. Zafra, A.E. Absalón, D.V. Cortés-Espinosa, Morphological changes and growth of filamentous fungi in the presence of high concentrations of PAHs, Braz. J. Microbiol. 46 (2015) 937–941.

[22] W. Qiao, Y. Zhang, Z. Xie, Y. Luo, X. Zhang, C. Sang, S. Xie, J. Huang, Toxicity of perfluorooctane sulfonate on Phanerochaete chrysosporium: growth, pollutant degradation and transcriptomics, Ecotoxicol. Environ. Saf. 174 (2019) 66–74.

[23] A. Kallimanis, S. Frillingos, C. Drainas, A.I. Koukkou, Taxonomic identification, phenanthrene uptake activity, and membrane lipid alterations of the PAH degrading Arthrobacter sp. strain Sphe3, Appl. Microbiol. Biotechnol. 76 (2007) 709–717.

[24] F.P. Chavez, F. Gordillo, C.A. Jerez, Adaptive responses and cellular behavior of biphenyl-degrading bacteria toward polychlorinated biphenyls, Biotechnol. Adv. 24 (2006) 309–320.

[25] A. Barman, D. Gohain, U. Bora, R. Tamuli, Phospholipases play multiple cellular roles including growth, stress tolerance, sexual development, and virulence in fungi, Microbiol. Res. 209 (2018) 55–69.

[26] J.T. Djordjevic, Role of phospholipases in fungal fitness, pathogenicity, and drug development – lessons from Cryptococcus neoformans, Front. Microbiol. 1 (2010) 125.

[27] R.W. Titball, Bacterial phospholipases, J. Appl. Microbiol. Symp. Suppl. 84 (1998) 1275–1375.

[28] C. Nakagawara, M. Arioka, Distinct enzymatic and cellular characteristics of two phospholipases A1 in Aspergillus oryzae, Biochem. Biophys. Res. Commun. 518 (2019) 644–650.

[29] Q. Zhu, B. Zhou, Z. Gao, Y. Liang, Effects of phospholipase C on Fusarium graminearum growth and development, Curr. Microbiol. 71 (2015) 632–637.

[30] J. Balsinde, Roles of various phospholipases A2 in providing lysophospholipid acceptors for fatty acid phospholipid incorporation and remodeling, Biochem. J. 364 (2002) 695–702.

[31] L.E. Sverdrup, F. Ekelund, P.H. Krogh, T. Nielsen, K. Johnsen, Soil microbial toxicity of eight polycyclic aromatic compounds: effects on nitrification, the genetic diversity of bacteria, and the total number of protozoans, Environ. Toxicol. Chem. 21 (2002) 1644–1650.

[32] M. Broniatowski, M. Binczycka, A. Wójcik, M. Flasiński, P. Wydro, Polycyclic aromatic hydrocarbons in model bacterial membranes – Langmuir monolayer studies, Biochim. Biophys. Acta 2017 (1859) 2402–2412.

[33] A. Wójcik, P. Perczyk, P. Wydro, M. Broniatowski, Incorporation of cyclodiene pesticides and their polar metabolites to model membranes of soil bacteria, J. Mol. Liq. 298 (2020), 112019.

[34] A. Wójcik, A. Bieniasz, P. Wydro, M. Broniatowski, The effect of chlorination degree and substitution pattern on the interactions of polychlorinated biphenyls with model bacterial membranes, Biochim. Biophys. Acta 2019 (1861) 1057–1068.

[35] R.W. Titball, C.E. Naylor, A.K. Basak, The Clostridium perfringens α-toxin, Anaerobe 5 (1999) 51–64.

[36] J.J. Virgen-Ortiz, J.C.S. dos Santos, C. Ortiz, A. Berenguer-Murcia, O. Barbosa, R. C. Rodrigues, R. Fernandez-Lafuente, Lecitase ultra: a phospholipase with great potential in biocatalysis, Mol. Catal. 473 (2019), 110405.

[37] P. Perczyk, M. Broniatowski, Simultaneous action of microbial phospholipase C and lipase on model bacterial membranes – modeling the processes crucial for bioaugmentation, Biochim. Biophys. Acta 1863 (2021), 183620.

[38] J.T. Davies, E.K. Rideal, Interfacial Phenomena, Academic Press, New York, 1961.

[39] I.S. Costin, G.T. Barnes, Two-component monolayers. II. Surface pressure—area relations for the octadecanol—docosyl sulphate system, J. Colloid Interface Sci. 51 (1975) 106–121.

[40] L.K. Nielsen, J. Risbo, T.H. Callisen, T. Björnholm, Lag-burst kinetics in phospholipase A2 hydrolysis of DPPC bilayers visualized by atomic force microscopy, Biochim. Biophys. Acta 1420 (1999) 266–271.

[41] Qi He, J. Li, Dynamic and morphological investigation of phospholipid monolayer hydrolysis by phospholipase C, Biochem. Biophys. Res. Commun. 300 (2003) 541–545.

[42] P. Høyrup, K. Jørgensen, O.G. Mouritsen, Phospholipase A2 – an enzyme that is sensitive to the physics of its substrate, Europhys. Lett. 57 (2002) 464–470.

[43] C. Stefaniu, G. Brezesinski, H. Möhwald, Langmuir monolayers as models to study processes at membrane surfaces, Adv. Colloid Interf. Sci. 208 (2014) 197–213.

[44] K. Kjaer, Some simple ideas on X-ray reflection and grazing-incidence diffraction from thin surfactant films, Phys. B 198 (1994) 100–109.

[45] J. Als-Nielsen, D. Jacquemain, K. Kjaer, F. Leveiller, M. Lahav, L. Leiserowitz, Principles and applications of grazing incidence X-ray and neutron scattering from ordered molecular monolayers at the air-water interface, Phys. Rep. 246 (1994) 251–313.

[46] P.J. Brennan, D.M. Losel, Physiology of fungal lipids: selected topics, Adv. Microb. Physiol. 17 (1978) 47–179.

[47] A. Felczak, P. Bernat, S. Różalska, K. Lisowska, Quinoline biodegradation by filamentous fungus Cunninghamella elegans and adaptive modifications of the fungal membrane composition, Environ. Sci. Pollut. Res. 23 (2016) 8872–8880.

[48] Y. Zhu, L. Wu, J. Zhu, Y. Xu, Q. Yong, S. Yu, Quantitative lipidomic insights in the inhibitory response of Pichia stipitis to vanillin, 5-hydroxymethylfurfural, and acetic acid, Biochem. Biophys. Res. Commun. 497 (2018) 7–12.

[49] P. Stolarek, S. Różalska, P. Bernat, Lipidomic adaptations of the Metarhizium robertsii strain in response to the presence of butyltin compounds, Biochim. Biophys. Acta 2019 (1861) 316–326.

[50] M.F. Renne, A.I.P.M. de Kroon, The role of phospholipid molecular species in determining the physical properties of yeast membranes, FEBS Lett. 592 (2018) 1330–1345.

[51] C.E. Martin, C.S. Oh, Y. Jiang, Regulation of long chain unsaturated fatty acid synthesis in yeast, Biochim. Biophys. Acta 1771 (2007) 271–285.

[52] S. Wagner, F. Patauf, Generation of glycerophospholipid molecular species in the yeast Saccharomvces cerevisiae. Fatty acid pattern of phospholipid classes and selective acyl turnover at sn-1 and sn-2 positions, Yeast 10 (1994) 1429–1437.

[53] A.I.P.M. de Kroon, P.J. Rijken, C.H. De Smet, Checks and balances in membrane phospholipid class and acyl chain homeostasis, the yeast perspective, Prog. Lipid Res. 52 (2013) 374–394.

[54] A. de Ghellinck, G. Fragneto, V. Laux, M. Haertlein, J. Jouhet, M. Sferrazza, H. Wacklin, Lipid polyunsaturation determines the extent of membrane structural changes induced by Amphotericin B in Pichia pastoris yeast, Biochim. Biophys. Acta 2015 (1848) 2317–2325.

[55] P. Díaz-Hellín, S. Gómez-Alonso, A. Borrull, N. Rozès, R. Cordero-Otero, J. Úbeda, Membrane lipid variability in Saccharomyces cerevisiae wine strains rehydrated in the presence of metabolic activators, J. Agric. Food Chem. 62 (2014) 8679–8685.

[56] D.A. Mannock, R.N.A.H. Lewis, T.P.W. McMullen, R.N. McElhaney, The effect of variations in phospholipid and sterol structure on the nature of lipid–sterol interactions in lipid bilayer model membranes, Chem. Phys. Lipids 163 (2010) 403–448.

[57] J. Loffler, H. Einsele, H. Hebart, U. Schumacher, C. Hrastnik, G. Daum, Phospholipid and sterol analysis of plasma membranes of azole-resistant Candida albicans strains, FEMS Microbiol. Lett. 185 (2000) 59–63.

[58] L.M. Solanko, D.P. Sullivan, Y.Y. Sere, M. Szomek, A. Lunding, K.A. Solanko, A. Pizovic, L.D. Stanchev, T.G. Pomorski, A.K. Menon, D. Wüstner, Ergosterol is mainly located in the cytoplasmic leaflet of the yeast plasma membrane, Traffic 19 (2018) 198–214.

[59] J. Malinsky, M. Opekarova, W. Tanner, The lateral compartmentation of the yeast plasma membrane, Yeast 27 (2010) 473–478.

[60] C. Walker, S. Ryu, C.T. Trinh, Exceptional solvent tolerance in Yarrowia lipolytica is enhanced by sterols, Metab. Eng. 54 (2019) 83–95.

[61] K.B. Hanson, D.J. Hoff, T.J. Lahren, D.R. Mount, A.J. Squillace, L.P. Burkhard, Estimating n-octanol-water partition coefficients for neutral highly hydrophobic chemicals using measured n-butanol-water partition coefficients, Chemosphere 218 (2019) 616–623.

[62] D. Muir, R. Lohmann, Water as a new matrix for global assessment of hydrophilic POPs, Trends Anal. Chem. 46 (2013) 162–172.
[63] D.T.H.M. Sijm, J. Middelkoop, K. Vrisekoop, Algal density dependent bioconcentration factors of hydrophobic chemicals, Chemosphere 31 (1995) 4001–4012.
[64] P. Wydro, M. Flasiński, M. Broniatowski, Does cholesterol preferentially pack in lipid domains with saturated sphingomyelin over phosphatidylcholine? A comprehensive monolayer study combined with grazing incidence X-ray diffraction and Brewster angle microscopy experiments, J. Colloid Interface Sci. 397 (2013) 122–130.
[65] A. Ivankin, I. Kuzmenko, D. Gidalevitz, Cholesterol–phospholipid interactions: new insights from surface X-ray scattering data, Phys. Rev. Lett. 104 (2010), 108101.
[66] M. Broniatowski, M. Urbaś, Interactions of two structurally related anionic phospholipids cardiolipin and phosphatidylglycerol with phospholipase A2. Langmuir monolayer studies, Biochim. Biophys. Acta 1859 (2017) 155–166.
[67] G. Brezesinski, H. Mohwald, Langmuir monolayers to study interactions at model membrane surfaces, Adv. Colloid Interf. Sci. 100–102 (2003) 563–584.
[68] W. Daear, M. Mahadeo, E.J. Prenner, Applications of Brewster angle microscopy from biological materials to biological systems, Biochim. Biophys. Acta 2017 (1859) 1749–1766.
[69] P. Perczyk, R. Gawlak, M. Broniatowski, Interactions of fungal phospholipase Lecitase ultra with phospholipid langmuir monolayers – search for substrate specificity and structural factors affecting the activity of the enzyme, Biochim. Biophys. Acta 1863 (2021), 183687.
[70] L. Albarano, V. Zupo, M. Guida, G. Libralato, D. Caramiello, N. Ruocco, M. Costantini, PAHs and PCBs affect functionally intercorrelated genes in the sea urchin Paracentrotus lividus embryos, Int. J. Mol. Sci. 22 (2021) 12498.
[71] Y. Yang, L. Pan, Y. Zhou, R. Xu, D. Li, Benzo[a]pyrene exposure disrupts steroidogenesis and impairs spermatogenesis in diverse reproductive stages of male scallop (Chlamys farreri), Environ. Res. 191 (2020), 110125.
[72] M. Fernandez Santiago, P. Lopez-Aparicio, M.N. Recio, M.A. Perez-Albarsanz, Effect of Aroclor 1248 and two pure PCB congeners on phospholipase D activity in rat renal tubular cell cultures, J. Biochem. Mol. Toxicol. 21 (2007) 68–75.
[73] O.G. Mouritsen, T.L. Andresen, A. Halperin, P.L. Hansen, A.F. Jakobsen, U. B. Jensen, M.Ø. Jensen, K. Jørgensen, T. Kaasgaard, C. Leidy, A.C. Simonsen, G. H. Peters, M. Weiss, Activation of interfacial enzymes at membrane surfaces, J. Phys. Condens. Matter 18 (2006) S1293–S1304.
[74] M. Niewerth, H.C. Korting, Phospholipases of Candida albicans, Mycoses 44 (2001) 361–367.
[75] T. Yoko-o, D. Ichikawa, Y. Miyagishi, A. Kato, M. Umemura, K. Takase, M. Ra, K. Ikeda, R. Taguchi, Y. Jigami, Determination and physiological roles of the glycosylphosphatidylinositol lipid remodelling pathway in yeast, Mol. Microbiol. 88 (2013) 140–155.
[76] K. Jasieniecka-Gazarkiewicz, K. Demski, I. Lager, S. Stymne, A. Banaś, Possible role of different yeast and plant lysophospholipid:acyl-CoA acyltransferases (LPLATs) in acyl remodelling of phospholipids, Lipids 51 (2016) 15–23.